Light Charged Particle Identification by Means of Digital Pulse Shape Acquisition in the CHIMERA CsI(Tl) Detectors at GSI Energies

L. Acosta, F. Amorini, R. Bassini, C. Boiano, G. Cardella, E. De Filippo, L. Grassi, C. Guazzoni, *Member, IEEE,* P. Guazzoni, M. Kiš, E. La Guidara, Y. Leifels, I. Lombardo, T. Minniti, A. Pagano, M. Papa, S. Pirrone, G. Politi, F. Porto, F. Riccio, F. Rizzo, P. Russotto, S. Santoro, W. Trautmann, A. Trifirò, G. Verde, P. Zambon, *Student Member, IEEE,* L. Zetta

***Abstract*–We report the results obtained by applying digital pulse shape acquisition and digital signal processing to the signals from CsI(Tl) scintillators read out by photodiodes at high incident energy (400 MeV/u). The digitized signals allows the discrimination of light charged particles by computing the Fast and Slow components and the Rise Time of the output pulses of the CsI(Tl). When the energies of the light charged particles exceed those corresponding to their ranges in CsI(Tl), the points related to the punching-through particles gather in the corresponding scatter plots giving rise to a cusp. The punching-through points are used as energy calibration points for the reaction products stopped in the CsI(Tl). The obtained results suggest that at relativistic beam energies it is possible to perform efficient discrimination in charge and mass of light charged particles by using the energy vs. rise time computation.**

Manuscript received November 10, 2011. The research leading to these results has received the main part of funding from the Italian Istituto Nazionale di Fisica Nucleare in the framework of the EXOCHIM experiment and also from European Community's Seventh Framework Programme (FP7 / 2007-2011) under grant agreement n° 227431.

L.Acosta, F.Amorini, F.Porto, F.Rizzo, P.Russotto, are with Laboratori Nazionali del Sud and Università di Catania-Dipartimento di Fisica e Astronomia - I-95123 Catania, Italy (telephone: +39095542111, e-mail: author@lns.infn.it).

R.Bassini, C.Boiano, P.Guazzoni, F.Riccio, L.Zetta are with Dipartimento di Fisica dell'Università degli Studi and INFN, Sezione di Milano, I-20133 Milano, Italy (telephone: +390250317249, e-mail: author@mi.infn.it).

G.Cardella, E.De Filippo, A.Pagano, M.Papa, S.Pirrone, G.Politi, G.Verde are with INFN, Sezione di Catania and Università - Dipartimento di Fisica e Astronomia, I-95123 Catania, Italy (telephone: +390953785321, e-mail: author@ct.infn.it).

L.Grassi is with Ruđer Bošković Institute, HR-10002 Zagreb, Croatia (telephone: +38514561111, e-mail: laura@lnr.irb.hr).

C.Guazzoni and P.Zambon are with Politecnico di Milano-Dipartimento di Elettronica e Informazione and INFN Sezione di Milano, I-20133 Milano, Italy (telephone: +390223996147, e-mail: Chiara.Guazzoni@mi.infn.it).

M.Kiš is with Physikalisches Institut der Universität Heidelberg, D-69120 Heidelberg, Germany and Ruđer Bošković Institute, HR-10002 Zagreb, Croatia (telephone: +496159710, e-mail: m.kis@gsi.de).

E.La Guidara is with Centro Siciliano Fisica Nucleare e Struttura della Materia, I-95123 Catania, Italy (telephone: +39095542111, e-mail: laguidara@lns.infn.it).

Y.Leifels and W.Trautmann are with GSI Helmholtzzentrum für Schwerionenforschung GmbH, D-64291 Darmstadt, Germany (telephone: +496159710, e-mail: author@gsi.de).

I. Lombardo is with INFN, Sezione di Napoli and Dipartimento di Fisica, Università di Napoli, I-80126, Napoli, Italy (telephone: +3908176836, e-mail: lombardo@na.infn.it).

T.Minniti, S.Santoro, A.Trifirò are with INFN, Gruppo Collegato di Messina and Dipartimento di Fisica, Università di Messina, I-98100 Messina, Italy(telephone: +390906765030, e-mail: author@unime.it).

I. Introduction

DETECTION and identification of Light Charged Particles (LCP), $Z \leq 4$, are key ingredients in designing modern large area detectors aimed at studying heavy ion reactions at intermediate energies. In nuclear physics experiments at intermediate energies the identification of charged products is implemented with Si-CsI(Tl) telescopes, as in the CHIMERA multidetector array [1] that represents the most powerful apparatus with its capability of detecting 94% of the total solid angle coverage and featuring energy discrimination and energy, mass and charge identification of the reaction products.

In the CHIMERA 4π-multidetector array the identification of mass and charge of the emitted products is carried out in detection cells made by large-area 25 cm^2 thin silicon detectors followed by thick CsI(Tl) scintillators each coupled with a photodiode. In our previous works [2-4] we investigated the applicability of Digital Pulse Shape Acquisition (DPSA) methods to a typical CHIMERA detection cell and we showed the feasibility of high-resolution particle identification by means of direct digitization of the output waveforms of the CHIMERA telescope preamplifiers. The identification of products stopping in silicon relies on energy and pulse rise time measurement for charge identification, and on time-of-flight techniques for mass identification. For products punching through the silicon detectors, the charge identification is based on the (ΔE, E) method and the isotopic identification of LCP on the computation of the Fast (F) and Slow (S) components of the CsI(Tl) signals, by means of a suitable modification of the two-gate method [5]. As it is well known, the time-dependence of the light output of a CsI(Tl) crystal, $L(t)$, is characterized by a combination of two components [6] that can be described by exponential functions with different time constants:

$$L(t) = L_1 \exp\{-t/\tau_f\} + L_2 \exp\{-t/\tau_s\} \quad (1)$$

where L_1 and L_2 are the light amplitudes for the Fast and Slow components respectively, with time constants 0.4 μs ≤ τ_f ≤ 0.7 μs and τ_s up to 6 μs. The Fast component depends on the mass, charge and energy of the detected particle, as well as the relative intensity L_1/L_2, while the Slow component shows only

a moderate dependence on the particle type. This dependence is the basic feature that permits particle identification by the widely used pulse shape discrimination technique. The performed tests have proven that DPSA gives better results than standard analog electronics, while reducing the complexity of the electronic chains and acquisition system.

In this paper we show the results obtained by applying digital signal processing, specifically by computing the CsI(Tl) signal rise time, to the waveforms acquired from CHIMERA Si-CsI(Tl) telescopes using a ^{96}Zr beam at 400 MeV/u on a ^{96}Zr target.

II. The Experiment

A. Experimental Setup

The results here presented, acquired in May 2011 in the framework of the ASY-EOS experiment [7], are part of a large program undertaken with four CHIMERA wheels at GSI in Darmstadt in order to study the asymmetry term of the Equation of State of the Nuclear Matter [8].

The ASY-EOS experiment is focused on the measurement of direct and elliptic flows of neutrons, protons, and light complex particles in reactions of isospin asymmetric systems neutron rich, as: ^{197}Au + ^{197}Au, ^{96}Ru + ^{96}Ru and ^{96}Zr + ^{96}Zr at 400 MeV/u. The results will provide quantitative information on the density dependence of the symmetry energy at densities larger than the saturation one.

In the experimental setup – shown in Fig.1 – the LAND calorimeter is used for neutron and charged particle detection and is set at the polar angle θ_{lab} = 46.2°, in order to cover the midrapidity kinematic region for suitably-high transverse momenta. Kinetics energies are obtained from the measured time of flight.

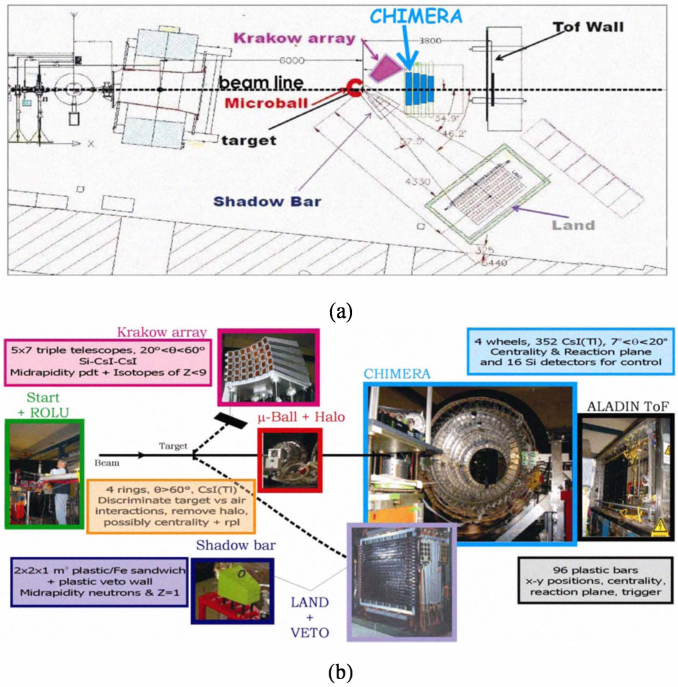

Fig. 1. Experimental setup of ASY-EOS experiment in Cave C at GSI. (a) top view. (b) scheme of principle with indication of main detector components and their role in the experiment.

The modulus of the impact parameter and the orientation of the reaction plane are determined by measuring the atomic number Z and the azimuthal direction for fragment emission at small angles, by means of a detection system with high effective granularity at forward angles, consisting of four wheels of the CHIMERA multidetector (352 CsI(Tl) scintillators, 16 of which equipped with 300 μm thick silicon detectors) and the ALADIN time of flight wall. In addition the flow of light fragments is measured with the Krakow triple telescope (Si + thin CsI(Tl) + thick CsI(Tl)) array at angles $\theta_{lab} > 30°$. Since the experiment is running in air, an additional hodoscope, the microball, positioned at backward angles, is used to identify interactions of the incident beam with air.

B. Digital Pulse Shape Acquisition

The presented tests have been performed by applying DPSA to collect the entire pulse waveform from the Si-CsI(Tl) telescopes of the CHIMERA wheels. The DPSA is achieved by means of high-resolution fast Sampling Analog to Digital Converters (SADC). The experimental setup is based on SADC VME-boards, directly connected through the VME-PCI Bridge to a host PC, used as supervisor [9], located in the controlled area, near to the detectors, and remotely controlled, via VNC software, by another PC, located in the acquisition room, responsible of data visualization and optionally off-line Event Parameter reconstruction. The electronic chain is constituted only by preamplifiers [10, 11], followed by antialiasing amplifiers [12]. The trigger signal used is the same as for the main acquisition of the ASY-EOS experiment.

With regards to the general philosophy we have enhanced the importance of the on board computation, in order to reduce the data traffic on VME bus and Bridge. The used VME-boards are able to perform online calculations and consequently Event Parameter reconstruction.

1) Hardware Architecture

In the present configuration, the digital pulse shape acquisition and on-board signal processing system is composed of:

- SADC acquisition and computation boards;
- VME-PCI optical-fiber bridge;
- host PC used as supervisor;
- additional PC used for results visualization.

The boards are SIS3150 VME-boards [13] (SIS3150) equipped with two ADSP-TS101S TigerSHARC Digital Signal Processors (DSPs) [14], 64 MB SDRAM memory, and two mezzanine sites for each board. A SIS9300 Card [15] is mounted on each of the mezzanine sites. Each SIS9300 provides four 14-bit, 100 MSample/s SADCs with programmable offset. Every time a trigger signal occurs, the pulse waveforms from all the four channels are collected.

The TigerSHARC ADSP-TS101S DSP is built with a static superscalar architecture and runs at a clock speed of 250 MHz executing up to four instructions per clock cycle. It has an internal 6-Mbit memory divided into three 2-Mbit blocks, each with its own 128-bit synchronous bus.

In the present tests, we used five SIS3150 boards, each one with two SADC mezzanines for a total of 8 SADC per board. We collected signals from 32 CsI(Tl) scintillators (8 per wheel) and also from some Silicon detectors. Furthermore we sampled the trigger pulse-shape for control purposes.

The pulses are acquired as waveforms of 2048 consecutive samples collected at 20 ns time intervals and stored in the SADC memory banks in wraparound mode. In this way the SADC continuously samples and stores the values into a circular buffer. Moreover the SIS9300 board has been used in post-trigger mode, to save also a part of the signal collected before the arrival of the trigger. This allows the baseline reconstruction exploiting about 500 samples before the pulse arrival and therefore the compensation, pulse by pulse, of long-term variations in the reference levels.

2) Software Architecture

The DAQ system features a modular architecture. Different custom codes have been written, each performing a different task. The first code runs on the DSPs of the SIS3150 boards. It controls the acquisition of the pulse-shape digital samples from the SIS9300 CMCs boards, and performs the on-line computation as desired. This program has been developed with Analog Devices' VisualDSP++ 4.0 [16] using the C++ language. An acquisition queue for storing incoming pulse shapes is kept by each DSP. Every time an event occurs, a trigger signal is delivered to the SIS9300 boards triggering the stop acquisition logic. At the same time, an interrupt is raised on the DSP1. The interrupt service routine waits for the acquisition to complete (a few μs) and then reads the event from the SIS9300 memory and stores it in one of the acquisition queues (if all acquisition queues are full, the event is lost), then the acquisition is restarted. On both DSPs, the queue is continuously checked for incoming pulse waveforms, and as soon as one is found, it is processed according to the user's settings. The pulse waveforms and the computed parameters are then stored in a cyclic sequence of output buffers in the SIS3150's memory. These buffers, when marked as full, will be read using the VME bus.

The on-board computation allows avoiding the transfer of the entire waveform to the host PC through the VME bus, removing the main bottleneck that impairs the acquisition rate in digital pulse shape acquisition systems. The pulse waveforms are transferred only if it is desirable to perform further off-line analyses (e.g. further improvements of the algorithms) or for diagnostic purposes. Even in this case, it is possible to apply a zero-suppression algorithm before transferring through the VME bus.

The other codes run on the host PC. One of them is devoted to the control of the SIS3150 boards through the VME-PCI bridge. Its task is to load the DSP software into the boards' RAM, setup the acquisition with the user-supplied parameters, and transfer the pulse shapes and the data computed on-board to the host PC, where they are saved to disk as a sequence of packets that can be read by other programs. It can work by polling continuously the boards under its own control, or by waiting for an interrupt to be delivered on the VME bus.

Data collected and saved by this code are used directly by a visualizer, written using the ROOT library [17] that can show the pulse waveforms and the event parameters computed by the DSPs, both on-line and off-line.

Furthermore, an off-line analysis program is used to obtain further event parameters from the saved pulse waveforms, or to compute again the same event parameters with different settings. In this case the algorithms used are identical to the ones used in the DSP and implemented in the same way, apart from trivial modifications due to the different architecture.

3) Algorithms

The event parameters used in this work are the Fast and Slow components and the Pulse Height and Rise Time for the signal coming from the scintillators. For signals coming from silicon only the pulse height is computed. The first step of the computation restores the baseline of the signal. The baseline part of the signal (i.e. the samples before the event trigger) is fit with a straight line that is extrapolated for the whole record length and subtracted from the digitized samples.

The signal is then filtered with a customizable FIR filter. The filter used in the present study is a triangular FIR of 87 tap length for the CsI pulses, while for the silicon pulses the tap length is 27. From this point on, the computation works on the filtered signal. We compute the signal amplitude as the value of the maximum collected sample. It provides an energy parameter dependent on the amount of energy released by the particle in the scintillator, and is used for the computation of the constant-fraction threshold values needed for the evaluation of the start time and the rise time of the signal. All the time values are computed using a Threshold Crossing Time (TCT) algorithm. The threshold value TV is computed as a predefined fraction of the maximum value. Then the algorithm selects the sample – pertaining to the rising edge of the pulse – whose value is nearest to the threshold value. A 3rd order polynomial $p(s)$, where s is the sample number, fits a given number of samples centered around the selected one in order to improve the precision. We obtain the fractional s_0 threshold-crossing sample – that is then converted into a time interval from the trigger – by solving the equation $p(s_0) = TV$. The rise time is computed as the difference between the crossing times of two user-defined thresholds, while the start time is computed as the crossing time of the 10% threshold. Owing to the sampling of the signals right at the output of the charge preamplifier, the computation of the Fast and Slow parameters relies on a modified version of the charge comparison method featuring very short computation time. In fact each parameter is computed as the difference between the sample values taken at the start and stop time of the corresponding time gate.

4) Computation Time

Several elements influence the execution time of the algorithms. In particular, the execution time of the TCT algorithm depends on the position of the sample crossing the threshold along the pulse waveform. The execution time of the

FIR filter is proportional to the number of taps in the filter kernel. Table 1 shows the execution times of several algorithms computed using the SIS3150 VME-Board and measured using the VisualDSP++ simulator. Note that the TCT algorithm is used once for computing the start time (used to fix the position of the Fast and Slow gates) and twice for computing the Rise Time.

The measured execution time for the processing of the CsI(Tl) pulses is, on average, about 0.6ms, using a 87 taps FIR filter. The dominant part of the computation time is due to the FIR filter, so we did not try to benchmark the Fast and Slow gate method against the rise time method with respect to the computing time. We chose instead to compute both methods in the same acquisition runs in order to compare their performance in particle discrimination capability.

III. Experimental Procedure and Results

A. Experimental Procedure

The waveforms have been used to reconstruct the (ΔE_{Si}, E_{CsI}) and (Fast, Slow) scatter plots exploiting the energy loss in the Silicon detector by the products crossing it and stopping in / crossing the CsI(Tl) crystal and the Fast and Slow components of the decay of the emitted light output. In order to reconstruct the (ΔE_{Si}, E_{CsI}) scatter plot we computed the maximum values of the waveforms at the output of the preamplifiers connected to the Si detector and to the photodiode reading the light output of the CsI(Tl). In order to reconstruct the (Fast, Slow) scatter plot we applied the two gate method to the waveforms from the CsI(Tl) scintillator.

The applied gates for the computation of the Fast and Slow components range between 0 and 600 ns for the Fast gate and between 900 ns and 6 μs for the Slow gate. The (Fast, Slow) scatter plot for the data collected by one of the 12 cm thick CsI(Tl) scintillator, is shown in Fig. 2.

Exploiting the dependence [18] of the decay constant τ_F associated with the Fast component on the ionization density for ion charges of $Z \leq 4$, $\tau_F \sim (dE/dx)^{-1} = f(E, Z, A)$, we investigated the possibility of particle identification plotting the rise time 30%-70% (RT) against the pulse height (PH_{CsI},).

As a comparison, in order to illustrate the particle identification capability of the rise time computation method, Fig. 3 shows the (PH_{CsI}, RT) scatter plot obtained using the same digitized waveforms of Fig. 2. The mass and charge identification is very sharp up to Z=3. In addition the hydrogen isotopes (p, d, t) and the ^{3}He and α particles are well separated.

TABLE I. Execution time of several algorithms computed using the SIS3150 VME-Board

Algorithms	Execution time (μs)
Baseline subtraction	39
FIR filtering (27 taps)	164
FIR filtering (87 taps)	445
Pulse Maximum search	17
Threshold crossing time	18
Rise Time	36
Fast and Slow components	0.1

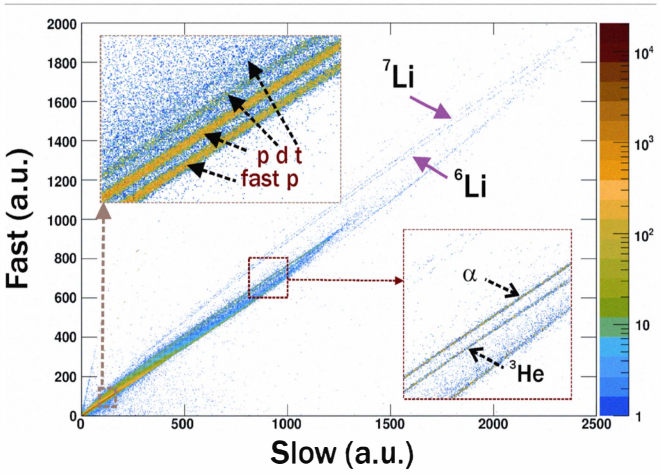

Fig. 2. (Fast,Slow) scatter plot for ^{96}Zr+^{96}Zr at 400 MeV/u.

Due to the finite thickness of the CsI(Tl) scintillator the most energetic light ions penetrate through it and a maximum amount of energy, varying with Z and A, is deposited in the crystal. When the energies of Z=1 and Z=2 isotopes exceed those corresponding to their ranges in 12 cm thick CsI(Tl) crystals, the punch-through points appear. The gathering of the points pertaining to punching-through particles creates a cusp in the corresponding cluster in the (Fast, Slow) scatter plot. As their energies increase, the corresponding isotope lines display a back-bending behavior.

A better representation of the (Fast, Slow) scatter plot data is achieved in Fig.4 where the height of the pulse is reported as a function of the Atan(Slow/Fast). In the scatter plots of Fig. 3 and Fig. 4 the punching-through energies are more prominent than in the usual (Fast, Slow) scatter plot, shown in Fig. 2. Therefore, these clearly visible punching-through points may be used as energy calibration points for the reaction products stopped in the CsI(Tl) scintillator, as described in the following subsection.

B. Energy Calibration

The SRIM code [19] allows computing the punch-through

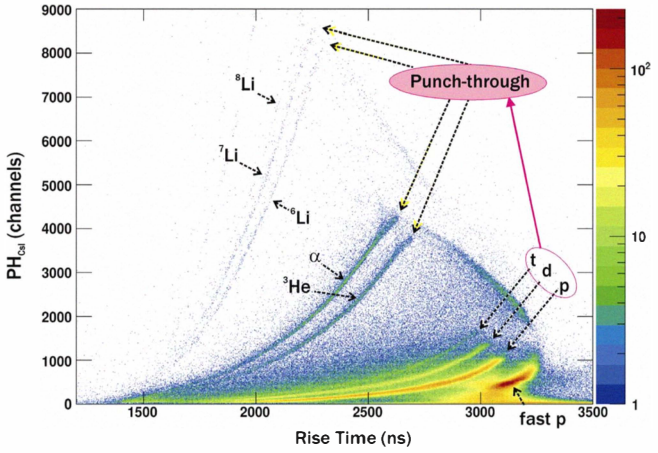

Fig. 3. (PH_{CsI},RT) scatter plot for ^{96}Zr+^{96}Zr at 400 MeV/u. The punch-through points for the different identified isotopes are indicated.

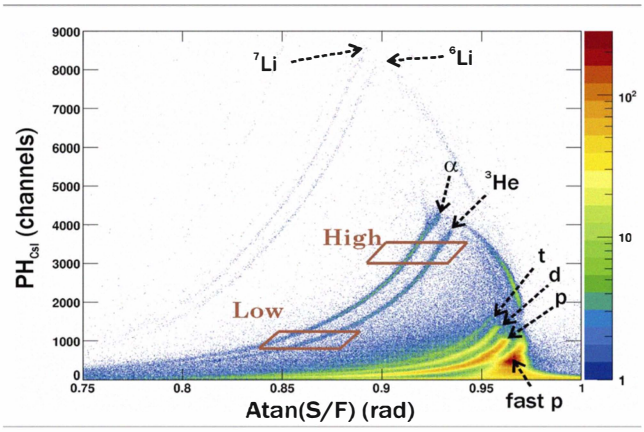

Fig. 4. (PH$_{CsI}$,Atan(S/F)) scatter plot for ^{96}Zr+^{96}Zr at 400 MeV/u.

energy of ions, whose projected range in CsI(Tl) scintillator is equal to 12 cm, i.e. the CsI(Tl) crystal thickness given by the manufacturer. Consequently it is possible to determine the energy lost in silicon by a particle of given A and Z. Fig. 5 shows the computed punch-through energies in MeV for Z = 1, 2, 3 isotopes versus the pulse heights in channels. The points beautifully lie on a straight line, as demonstrated by the linear fit with very good regression coefficient r.

Using the silicon detector thickness (300μm) given by the manufacturer and the SRIM code we determined the energy losses in MeV of the different ions at the punching-through point in channels, as shown in the (PH$_{CsI}$, RT) scatter plot of Fig.3. The linear correspondence between pulse height and energy in silicon detectors provides several calibration points which allow the determination of the energy losses in the silicon detector for each detected particle. To this end contours around each type of particle stopped in the telescope are applied to the Atan or RT scatter plots, in order to obtain in the (ΔE_{Si}, $E_{CsI(Tl)}$) scatter plot the corresponding $E\Delta E \approx AZ^2$ curve for Z = 1, 2, 3 isotopes, as shown in Fig. 6. The obtained $E\Delta E \approx AZ^2$ curves, corresponding to the profiles of the different ion clusters obtained with a density method, are calibrated by using the $\Delta E = f(E, A, Z)$ relation from the SRIM code for silicon, as shown in Fig.7. Since the function that relates the energy lost by a given particle in a given thickness of silicon to the particle energy (E_{inc}) is bijective, the particle energy can be calculated from the energy loss and then the energy deposited in the CsI(Tl) scintillator as $E_{CsI} = E_{inc} - \Delta E_{Si}$.

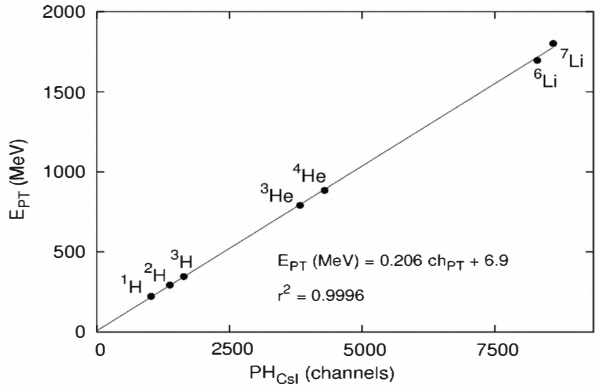

Fig. 5. Linear fit of the calculated punch-through energies in MeV to the corresponding CsI pulse heights in channels.

Fig. 8 shows the energy calibration for the CsI(Tl) scintillator obtained by linearly fitting the energy values obtained according to the aforementioned procedure. For sake of visibility, the CsI energy values are measured in MeV/u and shifted of the values (in MeV/u) indicated in parentheses.

C. *Results*

Fig. 3 and Fig. 4 clearly show the power of the (E, RT) and (E, Atan(S/F)) representations. In fact, the separation between protons and fast protons is very sharp, and the isotopic separation among Z = 1, 2, 3, 4 products is evident for all energies, even towards low particle energy. Moreover the punching-through points for all the products are well evidenced. In the scatter plot the fast proton cluster is due to high energy protons produced by the projectile fragmentation.

They have enough energy to punch through the CsI(Tl). The identification of this proton cluster is crucial in experiments at very high beam energies. Indeed, Z = 1, 2 isotopes emitted in the quasi-projectile fragmentation can provide important experimental information on the Equation of State (EOS) of the nuclear matter. Their identification could contribute to the knowledge of the asymmetry term of the EOS [20].

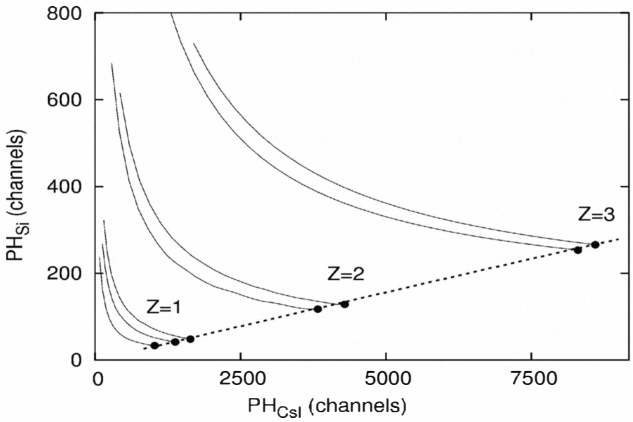

Fig. 6. $E\Delta E \approx AZ^2$ curves for Z=1, 2, 3 isotopes (see text). The punch-through points are highlighted.

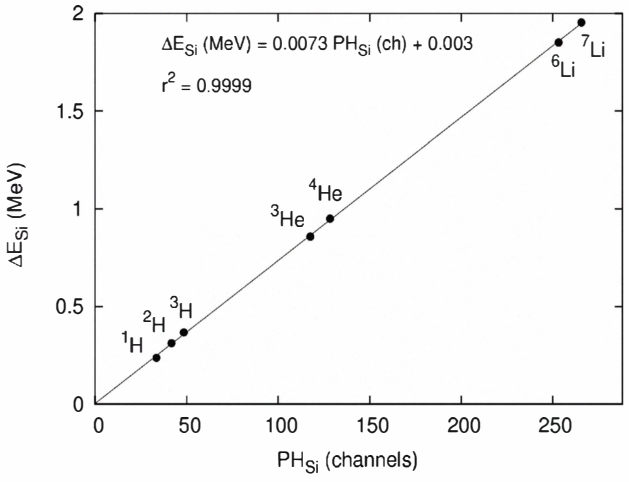

Fig. 7. Silicon detector linear energy calibration obtained by means of the indicated punch-through points energy values.

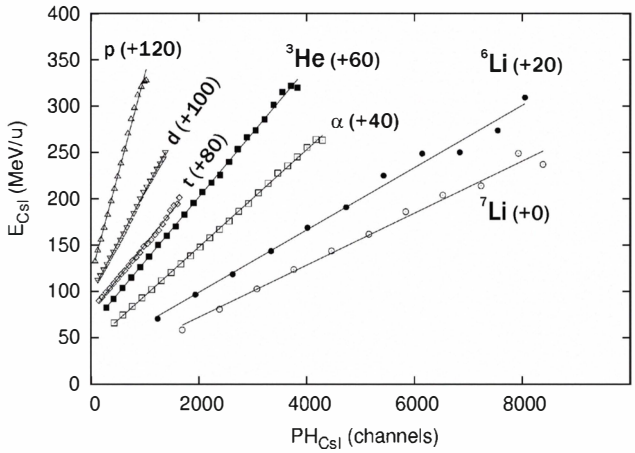

Fig. 8. CsI(Tl) scintillator energy calibration (see text).

In order to compare the LCP separation power of the three different representations of the collected data, we computed the Figure of Merit (FoM) [21] for pulse heights pertaining to two different bins (Low and High) of Z = 1 (p, d), Z = 2 (^{3}He, α) and Z = 3 (^{6}Li, ^{7}Li) isotopes. In Fig. 4 the Low and High bins – equal for the three different representations (see Table II) – are indicated for Z = 2. The FoM is defined as the separation between two peaks, i.e. the distance between their centroids, divided by the sum of their Full Width at Half Maximum. In order to compute the FoM in the chosen scatter plot, we select an area (A), delimited by two line-segments traced following the maximum-density lines of each of the considered isotope cluster. This area is transformed by means of an additional parameter, which is computed as the parametric coordinate of each event along the horizontal line joining the two segments, so that a point lying on the first segment has parametric coordinate *0* and a point lying on the second segment has parametric coordinate *1*. As an example Fig.9 shows the procedure for the (PH_{CsI}, RT) scatter plot.

In this way the selected portions of the isotope clusters are mapped to almost vertical clusters (B). This provides a natural choice for the identification axis which is obtained by projecting the scatter plot in the transformed coordinate system. The FoM is computed on the resulting histogram (C). In Table II the values of the computed FoMs of different pairs of isotopes for all the three used representations and two

TABLE II. FOM VALUES FOR DIFFERENT LCPS AND REPRESENTATIONS

Products	Pulse Height Bin	FoM RT	FoM Atan	FoM F/S
p,d	Low	1.18	1.29	1.31
	High	2.25	1.31	1.36
^{3}He,α	Low	2.04	2.04	2.14
	High	3.99	3.41	3.59
^{6}Li,^{7}Li	Low	2.51	3.37	3.17
	High	4.22	3.69	2.65

different pulse height bins, are shown. For the pair (p, d) the Low and High bins correspond to 300 - 400 and 800 - 900 channels, respectively. For the pair (^{3}He, α) the Low and High bins correspond to 900 - 1200 and 3000 - 3500 channels, respectively. For the pair (^{6}Li, ^{7}Li) the Low and High bins correspond to 3000 - 4000 and 6000 - 7000 channels, respectively.

IV. SUMMARY

In the present contribution we report the results obtained by applying digital signal processing to the waveforms collected from CsI(Tl) coupled to photodiodes, at relativistic energies. The measurement has been performed by studying reactions induced by a ^{96}Zr beam at 400 MeV/u on a ^{96}Zr target at GSI. The DPSA system is composed of a SADC SIS3150 VME-board, equipped with two ADSP-TS101S Tiger SHARC DSPs, 64 MB SDRAM memory and two mezzanine sites, each one carrying a SIS 9300 SADC Custom Mezzanine Card. The digitized signals have been used for discriminating LCP by computing for the CsI(Tl) signals the Fast and Slow components, the Atan(S/F) and its Rise Time by means of the TCT algorithm. The energy calibration of the Si-CsI(Tl) telescope is performed by exploiting for the punch-through points the different identified particles, as evidenced in the (PH_{CsI}, RT) scatter plot of Fig. 3, and by calculating the corresponding energies by means of the SRIM code. The shown results demonstrate that it is possible to perform an efficient discrimination of LCPs in charge and mass using the CsI(Tl) + photodiode combination and performing both Rise Time and Atan(S/F) computation. This is particularly the case of large dynamic ranges, typical of high energy measurements such as the one performed at 400 MeV/u.

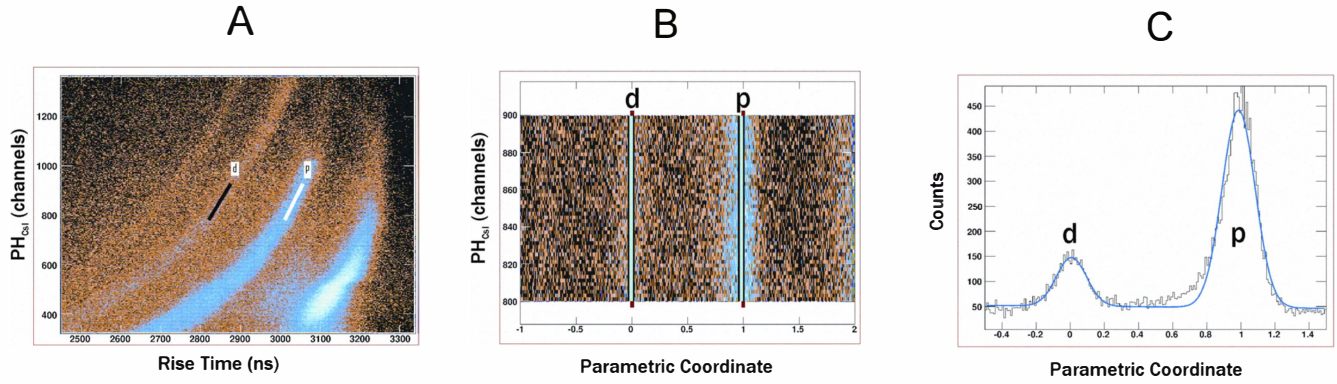

Fig. 9. For the pair p and d (High Energy bin) of the (PH_{CsI}, RT) scatter plot, the selected area (A), the vertical transformed selected portion (B), and the projection of the selected portion in the transformed coordinate system (C) are shown.

REFERENCES

[1] A. Pagano et al., "Physics with the CHIMERA detector at LNS in Catania: The REVERSE experiment", *Nucl. Phys.*, vol. A681, pp. 331c-338c, 2001.

[2] M. Alderighi, et al., "CHIMERA data acquisition via digital sampling technique", *IEEE Trans. Nucl. Sci.*, vol. 51, no. 4, pp. 1475 - 1481, 2004.

[3] M. Alderighi et al., "Charge identification in large area planar silicon detectors, using digital pulse shape acquisition", *IEEE Trans. Nucl. Sci.*, vol. 53 no. 1 pp. 279-285, Feb 2006.

[4] F. Amorini et al, "Digital Signal Processing for Mass Identification in a 4pi-Detector, Using Time of Flight Measurement", *IEEE Trans. Nucl. Sci.*, vol. 55, no. 3, pp. 717-722, Apr. 2008.

[5] D. Guinet, B. Chambon, B. Cheynis, A. Demeyer, D. Drain, and X. C. Hu, et al., "Using the combination CsI(Tl) and photodiode for identification and energy measurement of light particles", *Nucl. Instrum. Meth. A*, vol. 278, no. 2, pp.614 - 616, 1989.

[6] F. Benrachi et al., "Investigation of the performance of CsI(Tl) for charged particle identification by pulse-shape analysis", *Nucl. Instr. and Meth. A*, vol. 281, pp. 137-142, 1989.

[7] http://www.ct.infn.it/asyeos2010, R.C. Lemmon et al., Proposal for SIS Experiment S394 (2009), unpublished.

[8] W. Trautmann et al., "Differential neutron-proton squeeze-out", *Prog. Part. Nucl. Phys.*, vol. 62, pp. 425-426, 2009.

[9] P. Guazzoni *et al.*, "Proposed object-oriented architecture of a flexible small-scale system for digital pulse shape acquisition," *IEEE Trans. Nucl. Sci.*, vol. 53, no. 3, pp. 886–892, Jun. 2006.

[10] C. Boiano, R. Bassini, A. Pullia, A. Pagano, "Wide-Dynamic-Range Fast Preamplifier for Pulse Shape Analysis of Signals From High-Capacitance Detectors", *IEEE Trans. Nucl. Sci.*, vol. 51, no. 5, pp. 1931-1935, Oct. 2004.

[11] C. Boiano et al., "A ultra fast hybrid charge-sensitive preamplifier for high-capacitance detectors", *Nuclear Science Symposium Conference Record,* vol. 1, pp. 338-339, 2007.

[12] C. Boiano et al., "A 16-channel programmable antialiasing amplifier", *Nuclear Science Symposium Conference Record,* pp. 1389-1391, 2010.

[13] SIS 3150 VME CMC Carrier User Manual, SIS GmbH, Hamburg, Germany.

[14] ADSP-TS101S- Data Sheet, Norwood, Ma, Jan. 2005, Analog Devices, Inc.

[15] SIS 9300 ADC CMC User Manual, SIS GmbH, Hamburg, Germany.

[16] VisualDSP++ version 4.0 - User's Guide, Analog Devices Inc., Norwood, MA, U.S.A.

[17] R. Brun and F. Rademakers, "ROOT – An Object Oriented Data Analysis Framework", *Nucl. Instrum. Meth. A*, vol 389, pp. 81-86, 1997.

[18] T. Masuda et al., "The fluorescent decay of CsI(Tl) scintillator for charged particles of different ionization density", *Nucl. Instr. and Meth. A*, vol. 322, pp. 135-136, 1992.

[19] SRIM, the Stopping and Range of Ion in Matter - http://www.srim.org

[20] M. B. Tsang et al., "Constraints on the Density Dependence of the Symmetry Energy", *Phys. Rev. Lett.*, vol. 102, pp. 122701 (4 pages), 2009.

[21] R.A. Winyard et al., "Pulse shape discrimination in inorganic and organic scintillators", *Nucl. Instr. and Meth.*, vol. 95, pp. 141-153, 1971.